Title: **Phosphate removal and recovery from water using nanocomposite of immobilized magnetite nanoparticles on cationic polymer**

Ahmad Abo Markeb[a], Amanda Alonso[a,*], Antonio David Dorado[b], Antoni Sánchez[a], Xavier Font[a]

[a]Chemical Engineering Departament. Escola d'Enginyeria. Universitat Autònoma de Barcelona. 08193-Bellaterra (Spain)

[b]Universitat Politècnica de Catalunya, Av. Bases de Manresa, 61-73, 08242 Manresa, Barcelona (Spain)

*Corresponding Author: Amanda Alonso

amanda.alonso@uab.cat

Chemical Engineering Departament. Escola d'Enginyeria. Universitat Autònoma de Barcelona. 08193-Bellaterra (Spain)

Highlights

- Immobilization of magnetite nanoparticles on cationic polymer was synthesized.
- Phosphate removal using magnetite based nanocomposites was tested.
- Adsorption isotherms of phosphate at two pH; 5 and 7 were performed.
- Different isotherms models were applied for experimental data fitting.
- Regeneration and reusability of the magnetite based nanocomposites were carried out.

Graphical Abstract

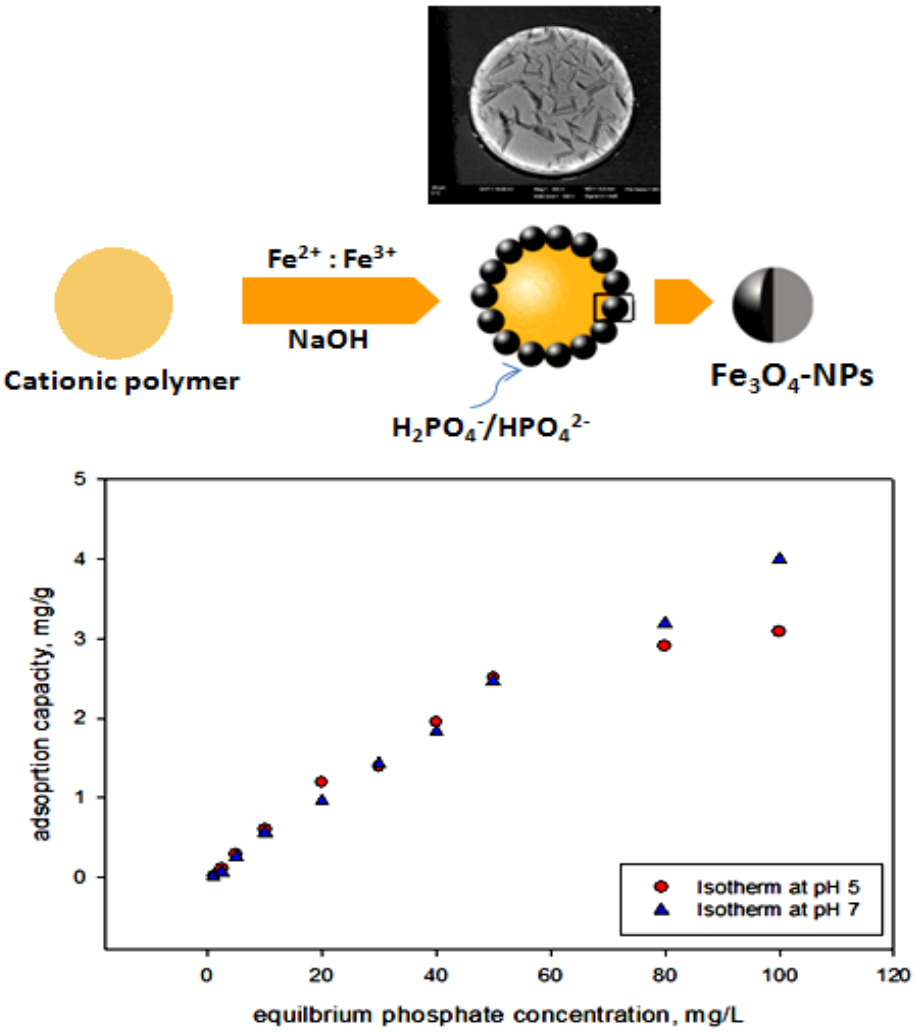

Abstract

A novel nanocomposite based on magnetite nanoparticles (Fe_3O_4-NPs) immobilized on the surface of the cationic exchange polymer, C100, using a modification of the co-precipitation method was developed to obtain magnetic nanocomposites (NCs) for phosphate removal and recovery from water. High resolution TEM-EDS, SEM, XRD, and ICP-OES were used to characterize the NCs. The continuous adsorption process by the so-called breakthrough curves was used to determine the adsorption capacity of the Fe_3O_4 based NC. The adsorption

capacity conditions were studied under different conditions (pH, phosphate concentration and concentration of NPs). The optimum concentration of iron in the NC for phosphate removal was 23.59 $mg_{Fe}/g_{NC.}$ The sorption isotherms of this material were performed at pHs 5 and 7. Taking into account the real application of this novel material in real water, the experiments were performed at pH 7, achieving an adsorption capacity higher than 4.9 $mg_{PO4\text{-}P}/g_{NC}$. Moreover, Freundlich, Langmuir and a combination of them fit the experimental data and were used for interpreting the influence of pH on the sorption and the adsorption mechanism for this novel material. Furthermore, regeneration and reusability of the nanocomposite were tested obtaining 97.5 % recovery of phosphate for the first cycle and at least 7 cycles of adsorption-desorption were carried out with more than 40% of recovery. Thus, this work described a novel magnetic nanoadsorbent with promoting properties for phosphate recovery in wastewater.

Keywords: magnetite nanoparticles; polymeric nanocomposite; adsorption; phosphate removal; wastewater

1. Introduction

Contamination of water is a widespread problem throughout the world as a result of pollution. Hence, wide range of pollutants, from organic pollutants such as pesticides [1], to metals such as hexavalent chromium [2, 3] and cadmium [4] in aqueous environment can be considered for remediation. Also, one of the most important pollutants in water is the excess of nutrients (nitrogen and phosphorus) that threatens human health and the environment. In particular, high amount of phosphorus promotes algae growth in water, since it is usually

regulated by microorganisms, which in its turn decreases oxygen concentration and leads to eutrophication (extraordinary growth of algae as a result of excess nutrients in water bodies) on rivers, lakes, and seas worldwide [5, 6]. Due to phosphorus is a non-renewable element and huge amount of phosphorus is lost annually for lack of phosphorus recovery, its recycling is of great interest especially with increasing demands, such as in the agriculture [7] as a fertilizer [8, 9] or industrial usages as ingredients for human food, pharmaceuticals, detergents, and food additive in the animal feed [10, 11]. Therefore, phosphorus is a critical element in water, where it was found frequently contained in groundwater, domestic and industrial wastewaters.

The common forms of phosphorus found in wastewater include phosphates ($H_2PO_4^-$, HPO_4^{2-}, and PO_4^{3-}), polyphosphates and organic phosphates [12]. Phosphorus concentrations in water matrices can be very different. For instance, municipal wastewater may contain 4-15 mg/L phosphorus as PO_4^{3-}, domestic wastewater contains about 10–30 mg/L of PO_4^{3-}, and treated sewage contains lower concentration, 1–5 mg/L of PO_4^{3-}. However, industrial wastewater (such as detergent manufacturing and metal coating processes) may contain phosphate levels of more than 10 mg/L [13]. Due to the potential interest of phosphate removal from water, various techniques have been employed, including constructed wetlands [14], physicochemical treatment method based on the precipitation of slightly soluble phosphorous [15], and biological nutrient removal (BNR) methods [9, 16, 17, 18, 19, 20, 21, 22]. Sludge used in BNR methods had disadvantages especially with a high phosphorous content due to there is a risk of phosphate release and flowing back to water treatment system if the aeration is not sufficient [23]. Thus, precipitation and activated-sludge process were studied for removing high concentration (hundreds to thousands of mg/L) [24] of phosphate

in wastewaters. However, in the case of low concentration (several mg/L) of phosphates, precipitation or activated-sludge method is not much effective [25]. For instance, the precipitation and crystallization methodologies present some disadvantages such as the requirement of pH higher than 9 to complete precipitation which have to disadvantages, as example, especially in the presence of carbonate/bicarbonate anions competitive interaction, difficult to regenerate and reuse which led to high cost for treatment. Other purification process performed on polluted water bodies, as high recovery reverse osmosis (RO) [9, 26], suffers problems associated with phosphate ions and in combination with calcium ions as precipitating agent for phosphate salts which lead to membrane blockage what limits water recovery [27].

Many challenges of the previous described water treatments were faced by the use of the nanotechnology that provides also cost effective treatment capabilities [28]. Nanomaterials have a number of key physicochemical properties that make them particularly attractive for water purification such as separation media or reusability. On a mass basis, they have much large surface areas than bulk particles. Nanomaterials can also be functionalized with various chemical groups to increase their affinity toward a given compound. They can also serve as high capacity - selectivity and recyclable ligands for toxic metal ions, radionuclides, organic and inorganic solutes [29]. Therefore water treatment based on the adsorption of contaminants using nanomaterials, such as cerium oxide or iron oxide- based nanoparticles, is relatively useful and cost effective method for water contaminants[30, 31, 32, 33, 34, 35, 36, 37, 38, 39, 40, 41, 42, 43] and also for phosphate removal [30, 31, 33, 34, 35, 36, 38, 39, 40, 41, 43]. Adsorption is generally used to remove organic [44] and inorganic contaminants such as heavy metals [45] from water and wastewater treatment.

Nanoadsorbents offer significant improvement with their extremely high specific surface area and associated sorption sites, short intra-particle diffusion distance, and tunable pore size and surface chemistry. In general, adsorption technology has been a well established technology for phosphate removal and recovery from water and wastewater, though more selective and cost effective sorbents developed. Compared with chemical precipitation, adsorption does not produce large volumes of chemical sludge. Various types of phosphorus adsorbents made from zeolites [46], lanthanum and yttrium compounds [47, 48], aluminum compounds [49, 50, 51, 52, 53], zero-valent iron [54], amine-functionalize, $Pr(OH)_3$ [55], magnesium amorphous calcium carbonate [56], zirconium compounds [57, 58], and iron(III) oxide compounds [12, 30, 31, 38, 40, 51, 59, 60, 61] were studied.

In addition to all of these nanoadsorbents, studies were also focused on the iron based adsorbents, with magnetic properties, due to their low cost [62] and their magnetic separation methodology which offers great advantages, such as high speed, simplicity, accuracy and effectiveness to operate as compared to the conventional separation methods [63]. Thus, magnetic nanoparticles (NPs) have a high potential to be applied in adsorption systems because they can easily be separated in a magnetic field. However, there are just a few studies of phosphate removal from water by using magnetite (Fe_3O_4) NPs [64, 65].

On the other hand, the modification of polymers with surface functional groups, such as acrylamide [66], N-vinylpyrrolidone [67] and also the modification of surfaces with magnetic properties have been reported. In this sense, polymeric ligand exchangers exhibit high phosphate selectivity over competing sulfate and chloride ions [16, 19] and efficient regeneration and reuse. However, they are relatively expensive, which is the most important parameter for the industrial applications. In this regard, the modifications of polymers or

other supports with NPs have been used recently [68, 69] to enhance the adsorption capacity of the materials. For instance, Hydrated Ferric Oxide (HFO) was doped in various support materials such as zeolites, alginates, activated carbon and cation exchange resins [70, 71, 72, 73] as well as in polymeric anionic exchanger [74, 75]. Anionic resins impregnated with HFO were studied for phosphorus removal [76, 77, 78, 79]. In general, polymeric anion exchange resins have low phosphate exchange capacity and poor selectivity factors against common ions present in wastewater (chloride, sulfate, bicarbonate, nitrate and dissolved organic matter) [19]. In this sense, other polymeric materials, such as the cation exchange resin, from Purolite (C100), is a simple, fast and economic polymeric matrix for the removal of metals such as Ce^{4+}, Fe^{3+}, and Pb^{2+} from aqueous systems [80]. Furthermore, taking into account some works reported about the use of iron-based nanoadsorbents for phosphorus removal in waters, it has been shown that the adsorption capacities at room temperature were: 0.3 mg/g for α-Fe_2O_3 [12], 0.9 mg/g for Goethite + Maghemite ($FeO(OH)$ + γ-Fe_2O_3) [81], 1.1 mg/g Hematite (Fe_2O_3) [82], and 2.6 mg/g for hydrothermally synthesized Fe_3O_4 [64]. However, higher adsorption capacities are required and no studies were conducted on the removal of phosphate based on cationic polymers and so far. Thus, iron based nanoadsorbents based on polymeric supports could be a promoting solution.

Therefore, this work aims to develop and use an optimal nanoadsorbent based on immobilized Fe_3O_4-NPs on the polymeric cationic resin, C100, for phosphate removal by adsorption and its recovery from water in a continuous fixed bed column. More precisely, the main objectives of this study are: 1) the optimization of the nanocomposite (NC) based on the immobilization of different Fe_3O_4-NPs concentrations on the surface of the C100 material to obtain the highest adsorption capacity for phosphate, and 2) the adsorption- desorption

optimization process to regenerate the adsorbent for the reusability of the NC and phosphate recovery during several cycles of usage.

2. Material and methods

2.1. Materials

Iron (II) chloride; $FeCl_2$, Iron (III) chloride hexahydrate; $FeCl_3.6H_2O$, sodium phosphate monobasic; NaH_2PO_4, citric acid and ammonium hydroxide, NH_4OH, were purchased from Sigma-Aldrich, Spain. Sodium hydroxide pellets, NaOH, was purchased from Merck. Hydrochloric acid, HCl, was purchased from Panreac, SA. All the chemicals were of analytical grade or higher, and all solutions were prepared with Milli-Q water and filtered using 0.45 µm Nylon membrane filter.

The cationic exchange polymer (C100) consists of polystyrene cross-linked with divenyl benzene functionalized with sulfonated group gel type and kindly supplied by Purolite S.A, Spain. The ion-exchange capacity (IEC) of the polymer was 2.0 mequiv/g.

2.2. Synthesis of the nanocomposite based on magnetite NPs

Pre-treatment of the C100 was carried out by following the procedure already described [83, 84]. First, the raw material was treated with 1.0 M NaCl for 2 h and washed with deionized water (3 times) so as to convert all the functional groups into Na^+ form. Afterwards, the resins were dried at 80ºC for 24 h.

Immobilization of the Fe_3O_4-NPs on the polymeric matrix, C100, was carried out using a variation of the Intermatrix Synthesis (IMS) protocol coupled to a co-precipitation method already reported [83].

The experimental procedure for the preparation of iron oxide based ferrites involves the precipitation of Fe^{2+} and Fe^{3+} salts in a strict ratio of 1:2 in deoxygenated water by the addition of a strong basic solution, in this work, NaOH, at 40°C under N_2 as an inert atmosphere (Equation 1).

$$Fe^{2+} + 2Fe^{3+} + 8OH^- \rightarrow Fe_3O_4 + 4H_2O \quad \text{(Eq. 1)}$$

Specifically, 125 mL of deoxydenated aqueous solution of NaOH 0.5M was added slowly with continuous stirring into 100 mL mixture of deoxygenated iron salts suspension, with Fe^{2+}/Fe^{3+} molar ratio of 1:2, which contained 0.4 g of C100 polymer under N_2 atmosphere and at 40°C. To optimize the concentration of NPs on the surface of polymeric cationic resin, we have used four different concentrations of $FeCl_2/FeCl_3$. These are: protocol A: 26/52 mM, protocol B: 13/26 mM, protocol C: 6.5/13 mM and protocol D: 3.25/6.50 mM. Then, the suspension was incubated for 1h at 40 ºC. During the incubation, the polymer became black in colour due to the formation of Fe_3O_4-NPs on the polymeric material. The IMS of Fe_3O_4-NPs in sulfonated polymers can be described by Equations 2 and 3 [85].

$$8(R\text{-}SO_3^-Na^+) + Fe^{2+} + 2Fe^{3+} \rightarrow (R\text{-}SO_3^-)_2(Fe^{2+}) + 2[(R\text{-}SO_3^-)_3(Fe^{3+})] + 8Na^+ \quad \text{(Eq.2)}$$

$$(R\text{-}SO_3^-)_2(Fe^{2+}) + 2[(R\text{-}SO_3^-)_3(Fe^{3+})] + 8NaOH \rightarrow 8(R\text{-}SO_3^-Na^+) + Fe_3O_4 + 4H_2O \quad \text{(Eq.3)}$$

2.3. Characterization of the nanocomposites

2.3.1. Inductively coupled plasma optical emission spectrometry, ICP-OES

The metal content of the NC samples was analyzed by using ICP-OES, Perkin Elmer model Optima 4300DV. The pre-treatment of the samples consists of an acid digestion, dilution and filtration using 0.45 μm Nylon filters. The metal amount was reported in terms of mg_{Fe}/g_{NC} (where g_{NC} refers to the mass of the NCs). Analyses were performed at Servei d'Anàlisi Química, Universitat Autònoma de Barcelona (UAB), Spain.

2.3.2. X-Ray Diffraction, XRD

XRD technique was used to obtain the crystalline structure of the particles. In a diffraction pattern, the location of the peaks on the 2θ scale can be compared to reference peaks. Diffraction patterns were collected on Panalytical X´Pert PRO MPD (Multipurpose Diffractometer). Analyses were performed at Institut Català de Nanociència i Nanotecnologia (ICN2), Spain. The identification of magnetite was based on the characteristic peaks in the diffractograms and comparing with the database.

2.3.3. Scanning Electron Microscopy and Energy-Dispersive Spectroscopy, SEM-EDS

Zeiss Merlin with a Field Emission microscope from Servei de Microscopia at UAB was used to study the cross-sectioned NCs samples. Cross sections were obtained by embedding the NC in epoxy resin and then, cross- sectioning with a Leica UC7 ultramicrotome (using a 35° diamond knife from Diatome) used to obtain the metal concentration profiles along the materials. EDS measurements were acquired with an Oxford INCA X-MAX detector [85].

2.3.4. Transmission Electron Microscopy, TEM

JEM-2011/ JEOL microscope from Servei de Microscopia at UAB was used to characterize the cross-sectioned of Fe_3O_4-NPs on the NC. The samples were embedded in epoxy resin for cross-sectioned analysis as described in SEM section (section 2.3.3).

2.3.5. Surface area measurements by Brunauer-Emmett-Teller method, BET

Surface area of dry resin and the NCs were determined from conventional nitrogen sorption isotherms at Institut Català de Materials Avançats de Barcelona (ICMAB), Spain, utilizing the BET theory. The instrument employed was a Micromeritics ASAP2000 with dedicated software.

2.4. Ionic chromatography (IC) for phosphate analysis

The determination of phosphate, as phosphorous (PO_4-P), was performed utilizing ICS-2000 (Dionex) ion chromatographic system, with ultimate 3000 autosampler. An ion exchange column specifically designed for rapid analysis of inorganic anion (Dionex IonPac AS18, 4 x 250 mm) equipped with an IonPac guard column (Dionex IonPac AG18, 4 x 50 mm) was used. Chromeleon® software was used to acquire data and control the instrumentation. Calibration standards and samples were filtered using 0.45 µm Nylon membrane filter before injection. Error in the measurements is < 1.2%.

2.5. Adsorption-desorption tests

2.5.1. Phosphate solutions

Phosphate solutions were prepared using a Na_2HPO_4 stock solution of 10000 mg/L in milli-Q water. Then, series of dilutions with a range of concentration from 0.1 to 100 mg/L of phosphate in milli-Q water were prepared for calibration. Each solution was filtered using 0.45 µm nylon membrane filter prior to analysis. When necessary, different pH was adjusted using 0.1 M citric acid or 0.1M sodium hydroxide.

2.5.2. Adsorption studies in a fixed bed column

The fixed bed column experiments were performed using polyamide column of 1 cm inner diameter and 16 cm length. The column was packed with the synthesized NC. A glass wool plug was placed at the bottom of the column to avoid the adsorbent washing out. Prior to start the experiment, the NC was fully wetted by pumping the column upwards for 4 hour with milli-Q water with flow rate 1mL/min. The flow rate was maintained in each experiment using a peristaltic pump (Watson Marlow, 403U).

The continuous adsorption process is usually characterized by the so-called breakthrough curves, i.e., a representation of the pollutant effluent concentration versus time profile in a fixed bed column. In addition, breakthrough curves prediction through mathematical models is a useful tool for scale-up and design purposes [86].

Breakthrough curve determination experiments were performed for all the experiments at 1 mL/min and 1.0 g of adsorbent (NCs).

The breakthrough curves show the loading behavior of phosphate to be removed from solution in a fixed-bed column and are usually expressed in terms of adsorbed phosphate as PO_4-P concentration (C_{ad}) as a function of time. Equilibrium uptake q_{eq} ($mg_{PO4\text{-}P}/g_{NC}$) is defined as the adsorption capacity of phosphate per mass of NC at a certain initial phosphate

concentration [87]. In all experiments, the initial concentration for phosphate was 10mg/L. Different pHs of the phosphate media were also evaluated of the pH range from 4 to 7 to evaluate the effect of the pH on the adsorption capacity as well as to evaluate the NC stability after the adsorption experiments.

2.5.3. Phosphate adsorption isotherm and modeling

To estimate the maximum adsorption capacity of the adsorbent, isotherm modeling is an important aspect for establishing adsorption system which provides information on the amount required for removing unit mass of pollutant. In this study, isotherms were performed continuously with phosphate interval concentrations (1, 2.5, 5, 10, 20, 30, 50, 80 and 100 mg/L), 1 g/L of nanoadsorbent, 1 mL/min at room temperature and two pH values; 5 and 7.

The experimental quantities of the phosphate adsorbed have been fitted to adsorption isotherms models available in the literature, including two-parameter isotherms (Langmuir, Freundlich, Dubinin–Radushkevich, DR), three-parameter isotherms (Brunauer–Emmett–Tellerand, BET) and a combination of them. Isotherms were determined from the breakthrough curves of step changes in the feed concentration by non-linear regression according to the value of the objective function defined as the norm of the difference between experimental data and model predictions. The sorption capacity of the material was evaluated at different pHs by frontal analysis following the stair case method [88]. Moreover, a confidence interval has been determined in the estimation of model parameters according to the Fisher information matrix method as function of the quantity and quality of experimental data [89].

Columns experiments started with 1 mg/L phosphate as initial concentration until equilibrium was reached. At that point, inlet phosphate concentration was increased

corresponding to the interval of phosphate concentration. For each initial phosphate concentration, q_{eq} was calculated.

2.5.4. Desorption of phosphate and reusability of the nanocomposite

The desorption process for the phosphate previously adsorb on the NC, as previously described, was optimized to be able to reuse the nanoadsorbent for further adsorption process and to recover the phosphate. To determine the optimal process for the adsorbent regeneration, different desorbing solutions, specifically NH_4OH, NaOH with different concentrations (0.01 – 1.0 M) and milli-Q water, were used. After 90 min adsorption of 10 mg/L phosphate solution at pH 7, 1mL/min and 1.0 g of the nanoadsorbent, aliquots of the NC (0.5 g of wetted adsorbent) were treated using the desorbing solutions. Once the optimal desorption system was defined, the adsorption-desorption processes were performed seven times at the optimal adsorption and desorption experimental conditions for evaluating the reusability of the synthesized NC for phosphate removal and its recovery.

3. Results and discussion

3.1.Synthesis and characterization of the nanocomposites

3.1.1. Metal ions content in the nanocomposites

The NCs, synthesized by using the four A, B, C and D, were analyzed by ICP-OES. Table 1 shows the mean of iron (Fe) concentration (mg_{Fe}/g_{NC}) for the three replicates of the four samples. It is shown that increasing the Fe salts concentration in the synthesis lead to increase the Fe

content in the final NC. Furthermore, data show that the Fe concentration on the polymer is saturated at around 80 mg_{Fe}/g_{NC} (samples A and B), being the maximum level of metal concentration during the synthesis of 13/26 mM of $FeCl_2/FeCl_3$ (for Protocol B).

(Table 1 here)

3.1.2. SEM-EDS, XRD and TEM analysis of the nanocomposites

The SEM images coupled with EDS of the cross-sections for each synthetic protocol (A, B and C) of the NCs are shown in Figure 1. This data shows the success of the immobilization of the Fe_3O_4-NPs on the surface of the NC. As it is clearly seen on Figure 1a, 1b, and 1c, the major part of the Fe_3O_4-NPs is located near the polymer surface (shown by the light white zone) with different thickness corresponding to each synthetic protocol showing a deeper layer when the loading concentration of iron during the synthesis is higher. Figure 1d shows cross section for polymer without NPs.

(Figure 1 here)

Further confirmation about the immobilization of magnetite NPs on the surface of the polymer was illustrated in Figure 1e, where the line spectrum shows the iron content profile obtained by SEM coupled with EDS, on the cross-sectioned of protocol C. It can be seen that the profile distribution of Fe presents a peak at the surface of the polymer meaning that the distribution of the Fe_3O_4-NPs is concentrated on the surface of the polymer which makes the material more suitable for its application as a nanoadsorbent. Furthermore, TEM images of the

cross-sectioned nanomaterials for protocol C is illustrated in Figure 2a. As it is observed, the NPs on the polymer show a size of 15 - 20 nm as it was also shown at [83]. Crystalline structure of Fe_3O_4-NPs was confirmed by electron diffraction pattern as shown in Figure 2b.

(Figure 2 here)

In addition, the X-ray diffractogram shows the crystalline structure of the pattern Fe_3O_4-NPs (Figure 3a), and the Fe_3O_4-NPs immobilized on the polymer before adsorption (Figure 3b). The typical peaks can be found at 35.5°, 43.0°, 57.1° and 62.7°, which preferably correspond to the Fe_3O_4 according to the JCPDS database [90]. The Miller indices of these peaks are 311, 400, 511 and 440, respectively. The broad peak in the XRD pattern could be attributed to the ultra fine nature and small crystallite size of magnetite nanocomposites, in addition to the formation of thin layer of magnetite nanoparticles immobilized on the surface of the cationic polymer. Moreover, the decrease of the intensity of the peaks could be attributed to the low concentration of iron contents [91, 92].

(Figure 3 here)

3.1.3. Magnetic characterization and surface area measurements of the nanocomposites

Figure 2c shows a photograph of the qualitative test of the magnetic properties of NC by using a permanent magnet, where one can clearly see the NC beads stuck to the magnet. This means that the NC material can be easily recovered from the medium for further reuse which is an advantage for the separation process in this application.

On the other hand, BET analysis reports that surface area for all protocols was lower than 2 m^2/g (N_2 sorption, BET). These results agree with the gel-type resins in the dry state that are

characterized by very low porosity and a far lower surface area, which usually does not exceed 5 m^2/g (N_2 sorption, BET) [93].

3.2.Adsorption studies in fixed-bed column

3.2.1. Determination of the adsorption capacities for the NCs with different Fe_3O_4-NPs content (Protocol A, B, C and D)

The influence of Fe_3O_4- NPs concentration in the NC on the adsorption capacities of 10 mg/L phosphate at pH 5 is shown in Table 1. The highest adsorption capacity was 3.62 $mg_{PO4\text{-}P}/g_{NC}$ obtained by using the material corresponding to Protocol C (23.59 ± 1.34 mg_{Fe}/g_{NC}) indicating that a higher concentration of NPs leads to a decrease of the adsorption capacity of the NC (as shown for Protocol A and B adsorption capacities, corresponding to 2.88 and 2.30 $mg_{PO4\text{-}P}/g_{NC,}$ respectively). This can be explained because an excess of NPs leads to decrease the surface/volume ratio of the NPs by the presence of aggregates or higher NPs size. On the other hand, protocol D did show an adsorption capacity lower than 0.01 $mg_{PO4\text{-}P}/g_{NC}$ (corresponding to the limit detection of the Ionic Chromatograph), which indicates that approximately less than 6.0 mg_{Fe}/g_{NC} had no significant effect on the NC for the adsorption process of phosphates like it is observed the adsorption capacity for C100 without NP. Thus, it was considered that protocol C (23.59 mg_{Fe}/g_{NC}) is the optimal iron content as well as NPs size and distribution in this NC for the adsorption of phosphates in water. Thus, the following experiments in this work and the majority of the characterization techniques used were carried out for sample C.

3.2.2. Effect of the pH on the adsorption capacities and on the nanocomposite stability

pH, as a critical water chemistry parameter, can significantly affect the adsorption of phosphate by any material. Figure 4 shows the adsorption capacities of 10 mg/L phosphate, as initial concentration, using Protocol C NC at a pH range from 4 – 7. Generally, phosphate has three pK_a values, 2.2, 7.2, and 12.3 which correspond to pK_{a1}, pK_{a2}, and pK_{a3} respectively, according to the presence of three species. HPO_4^{2-} and $H_2PO_4^-$ are the predominant species in the pH solution region between 4 and 10. HPO_4^{2-} is being more widespread in slightly alkaline conditions while $H_2PO_4^-$ in slightly acidic conditions [94]. As shown in Figure 4, in this study, the highest adsorption capacities value were at pH 7 indicating that the species involved in adsorption process are those which are related to the pK_{a2} value of 7.2. Thus, HPO_4^{2-} seems to have better affinity to form bidentate complexes with the magnetite NPs than $H_2PO_4^-$ forming M-OH^+ complex [95, 96, 97]. Moreover, when the pH<pK_a (as pK_{a2} in this case), the surface of the adsorbent is more positively charged and more efficient for attracting negatively charged phosphate species through electrostatic interaction. It is also reported that phosphate adsorption on the surfaces of other iron-based species (e.g. oxyhydroxide polymorphs goethite) is based on the formation of inner-sphere complexes between the phosphate anion and the iron oxyhydroxide surface, indicating the presence of Fe–O–P covalent bonds what it seems to be also contributing to the adsorption process in the system here reported [98].

Furthermore, the effect of pHs on the immobilized Fe_3O_4-NPs on the C100 after the adsorption processes described in Figure 4 was also determined by ICP-OES analysis to detect the stability of the NPs on the polymer for the adsorption mechanism. Thus, iron content after adsorption at different pHs showed the highest iron decrease at pH 4 of 43.4% while at pH 7 the decrease of iron content was 7% of the iron content. This decrease could be explained due to an oxidation of the iron present in the NPs that is finally released from the polymer. At the view of

these results pH 7 is the optimum pH for phosphate adsorption, due to both the highest adsorption capacity and the NC stability. Even more, adsorption process of 10 mg/L phosphate on the NC (protocol C) at pH 7 did not affect the crystalline structure (Figure 3c) of the NPs.

(Figure 4 here)

3.3.Adsorption Isotherms and modeling

Isotherm fitting results for the five different models tested are shown in Figure 5 up to a concentration of 100 mg/L. While in Figure 5a is observed that saturation conditions are achieved at pH 5, maximum capacity is not reached when material is operated at pH 7 (Figure 5b). These isotherms make it possible to accurately predict the experimental data (low fval) (Table 2). Wider confidence intervals are obtained in three-parameter isotherms in particular showing that a large number of possible combinations of parameters are able to fit model predictions to the experimental phosphate adsorbed on the materials. Thus, estimated parameters show a low sensitivity to the final result of the isotherm expression as in the case of BET isotherm. Thus, the Freundlich, Langmuir and the isotherm that combines three parameter-isotherms are the most suitable for fitting the experimental data and for interpreting the influence of pH on the sorption.

(Figure 5 here)

Freundlich isotherm is commonly used for describing sorption on heterogeneous surfaces. The n value indicates the degree of non-linearity between solution concentration and adsorptive material. As n value is lower than 1, the sorption process is more chemical than physical for both pHs. The estimated values of n are lower at pH 5 indicating that the behavior deviates in this case further from the linear isotherm, so it approaches a rectangular isotherm or irreversible isotherm. That means that the concentration needs to go down to an extremely low value before adsorbate molecules desorb from the surface. A higher value of this parameter at pH 7 reveals a weaker affinity between contaminant and material comparing with pH 5 results.

The higher value of Langmuir parameter K1 obtained for the isotherm at pH 7 underlines a higher sorption capacity of the material at these conditions (as also shown in Figure 4). The Langmuir isotherm assumes monolayer adsorption onto a surface containing a finite number of adsorption sites of uniform strategies with no transmigration of adsorbate in the plane surface. Once a site is filled, no further sorption can take place at that site. This indicates that at pH 5 the surface reaches a saturation point where the maximum adsorption of the surface is achieved. Since experimental data at pH 7 is not strictly following a saturation model as Langmuir, the maximum capacity of the material is an extrapolation that it should be checked if higher concentration than those tested in the present study are required. The higher value of k2 for pH 7 highlights again a lower affinity between material and contaminant compared to pH 5.

The Dubinin–Radushkevich isotherm equation, widely used for describing adsorption on microporous solids such as activated carbons, has a semi-empirical origin and is based on the assumptions of a change in the potential energy between the adsorbed phases and a characteristic energy of a given solid. Previous results are partially improved by means of the Redlich–Peterson isotherm. Unlike pH 5, sorption experiments conducted at pH 7 exhibits behavior similar to that of Henry's law, according to the parameter n, which is close to 0. In contrast, at the same range of phosphate concentrations, working a lower pH, the material reduce its capacity and reaches quickly saturation conditions.

From the modeling of the process, it is concluded that the kind of relationship set between contaminant and sorbent is described by a chemical interaction, as already mentioned in Section 3.2.2, through a Fe-OH complex system mechanism. While a pH 5, monolayer absorption reproduces more accurately the experimental behavior, saturation conditions are not achieved a pH 7. This means a stronger interaction at pH 5. Clearly, pH plays an important role in the affinity and capacities of materials when they are under adsorption conditions.

(Table 2 here)

The adsorption capacity of the magnetic nanocomposite for the removal of PO_4-P has been compared with various iron-based adsorbents in Table 3. The adsorption capacities of magnetite immobilized on C100 developed and tested in this work are much higher than other iron based nanoadsorbents but the one based on zirconium. However, the NC used in this work has an advantage in a real application pH medium and it is easier to recover than

the others ones. Therefore, the NC used in this study show highly competitive for phosphate removal.

(Table 3 here)

3.4.Evaluation of the phosphate recovery procedure and the reusability of the magnetite nanocomposite for several adsorption-desorption cycles.

It is known that at high alkaline pH, PO_4^{3-} species are the predominant in the solution medium and the magnetite is deprotonated and negatively charged, which is favorable for desorption of the adsorbed phosphate [74]. In this work, among the reagents used for the regeneration of magnetite based NC (protocol C), NaOH was found to be the most effective in desorbing the phosphate comparing to NH_4OH and Milli-Q water after one hour shaking at 200 rpm (31.5 and 12.6 % of phosphate recovered respectively). Further optimization procedure for desorbing process was performed using different concentration of NaOH. As shown in Figure 6 we can conclude that 0.5 M NaOH is the optimum concentration for desorption process. Under these conditions phosphates desorption was 52.9 %. Therefore, enhancement of desorbability percent was achieved by three washing cycles with 0.5 M NaOH to obtain 97.5 % of the phosphate recovered. This result is clearly interesting if ones compares with the recovered phosphate % reported in the literature (i.e. 40 % for phosphate for initial concentrations less than 100 mg/L [76]).

(Figure 6 here)

Afterwards, the regenerated magnetite NC was tested for reusability. After every adsorption process, desorption by using 0.5 M NaOH and three washing steps was performed. The results (Figure 7) showed that there is only a drop in the adsorption capacity after the 1st cycle, while the

efficiency of phosphate adsorption–desorption was nearly the same for the rest of six cycles. An explanation of the drop of the adsorption capacity after the first adsorption-desorption cycle could be explained by the loss of iron detected from ICP-OES analysis which was of 30% after the first cycle while remaining constant for the rest of cycles. The loss of the iron content from the NC could be due to the experimental conditions in which some of the iron ions dissolves in the media but the rest of the iron content remain stabilized in the polymeric matrix.

On the other hand, as mentioned, the recovery of phosphate was 97.5 % for the 1st cycle. A decrease on the recovery % was observed from the 1st to the 4th cycle of adsorption-desorption. After that, the recovery % removal remains constant at 45% approximately, as shown in Figure 7. In this sense, it could be confirmed the assumed adsorption mechanism (see section 3.2.2) in which a strong Fe-HPO_4 complex could be formed in each adsorption-desorption cycle and thus, avoiding the total recovery of the phosphate.

(Figure 7 here)

4. Conclusions

The present study provides magnetite nanoparticles immobilized on the surface of cationic polymer (C100) which displayed successful application to remove phosphate ions from aqueous solutions. Adsorption experiments of phosphate in a fixed-bed column using different concentrations of magnetite nanoparticles immobilized on the polymer proves that the optimum concentration of iron in the nanocomposites is 23.59 mg_{Fe}/g_{NC}. The effect of pH on the adsorption capacity showed a higher adsorption capacity from the optimized material at pH 7 comparing to pH 4, 5, and 6. Afterwards, continuous adsorption isotherms were

performed and it is shown a higher adsorption capacity (> 4.0 $mg_{PO4\text{-}P}/g_{NC}$) at pH 7 compared to pH 5 (2.8 $mg_{PO4\text{-}P}/g_{NC}$). Therefore, the magnetic nanocomposite used in this study is highly competitive for phosphate removal comparing to other iron-based nanoparticles reported in the literature. Furthermore, regeneration of the nanocomposite was optimized to obtain 97.5 % recovery of phosphate using 0.5 M NaOH for three consecutive cycles desorption process. Then, reusability was demonstrated for 7 cycle's adsorption-desorption process. Therefore we can conclude that the magnetite nanoparticles immobilized on the cationic polymer has great potential for adsorbing and recovering phosphate.

Acknowledgments

One of the authors, Ahmad Abo Markeb is grateful thanks the Ministry of Higher Education of Egypt for the Ph.D external mission. The authors would like to extend their gratitude to Purolite for kindly supply the cationic polymer.

References

1. Foo KY, Hameed BH. Detoxification of pesticide waste via activated carbon adsorption process. Journal of Hazardous Materials. 2010;175:1-11.
2. Mohan D, Pittman Jr CU. Activated carbons and low cost adsorbents for remediation of tri- and hexavalent chromium from water. Journal of Hazardous Materials. 2006;137:762-811.
3. Recillas S, Colón J, Casals E, González E, Puntes V, Sánchez A, Font X. Chromium VI adsorption on cerium oxide nanoparticles and morphology changes during the process. Journal of Hazardous Materials. 2010;184:425-31.
4. Contreras AR, García A, González E, Casals E, Puntes V, Sánchez A, Font X, Recillas S. Potential use of CeO2, TiO2 and Fe3O4 nanoparticles for the removal of cadmium from water. Desalination and Water Treatment. 2012;41:296-300.
5. Lau PS, Tam NFY, Wong YS. Wastewater Nutrients (N and P) Removal by Carrageenan and Alginate Immobilized Chlorella Vulgaris. Environmental Technology. 1997;18:945-51.
6. Trépanier C, Parent S, Comeau Y, Bouvrette J. Phosphorus budget as a water quality management tool for closed aquatic mesocosms. Water Research. 2002;36:1007-17.
7. Reijnders L. Phosphorus resources, their depletion and conservation, a review. Resources, Conservation and Recycling. 2014;93:32-49.
8. Sengupta S, Pandit A. Selective removal of phosphorus from wastewater combined with its recovery as a solid-phase fertilizer. Water Research. 2011;45:3318-30.
9. de-Bashan LE, Bashan Y. Recent advances in removing phosphorus from wastewater and its future use as fertilizer (1997–2003). Water Research. 2004;38:4222-46.
10. Kebreab E, Hansen AV, Strathe AB. Animal production for efficient phosphate utilization: from optimized feed to high efficiency livestock. Current Opinion in Biotechnology. 2012;23:872-7.
11. Vitti DMSSkE. Phosphorus and Calcium Utilization and Requirements in Farm Animals. Phosphorus and Calcium Utilization and Requirements in Farm Animals. 2010:1-178.
12. Zhu Z, Zeng H, Zhu Y, Yang F, Zhu H, Qin H, Wei W. Kinetics and thermodynamic study of phosphate adsorption on the porous biomorph-genetic composite of α-Fe2O3/Fe3O4/C with eucalyptus wood microstructure. Separation and Purification Technology. 2013;117:124-30.

13. Mezenner NY, Bensmaili A. Kinetics and thermodynamic study of phosphate adsorption on iron hydroxide-eggshell waste. Chemical Engineering Journal. 2009;147:87-96.
14. Prochaska CA, Zouboulis AI. Removal of phosphates by pilot vertical-flow constructed wetlands using a mixture of sand and dolomite as substrate. Ecological Engineering. 2006;26:293-303.
15. Ramadori R, di Pinto AC, Tandoi V, Sasso C. Chemical Precipation of Phosphate From Sewage At Low Lime Dosage. In: L. Pawlowski EMWJL, Sarzanini C, editors. Studies in Environmental Science. Volume 34: Elsevier; 1988. p. 223-33.
16. SenGupta A, Zhao D. Using a chelating ion exchange resin saturated with lewis acid, i.e., copper, cations. Google Patents; 2000.
17. Federation WE. Biological Nutrient Removal (BNR) Operation in Wastewater Treatment Plants: WEF Manual of Practice: McGraw-Hill Education; 2005.
18. Sedlak RI. Phosphorus and Nitrogen Removal from Municipal Wastewater: Principles and Practice, Second Edition: Taylor & Francis; 1991.
19. Zhao D, Sengupta AK. Ultimate removal of phosphate from wastewater using a new class of polymeric ion exchangers. Water Research. 1998;32:1613-25.
20. Isanta E, Figueroa M, Mosquera-Corral A, Campos L, Carrera J, Pérez J. A novel control strategy for enhancing biological N-removal in a granular sequencing batch reactor: A model-based study. Chemical Engineering Journal. 2013;232:468-77.
21. Carrera J, Vicent T, Lafuente J. Effect of influent COD/N ratio on biological nitrogen removal (BNR) from high-strength ammonium industrial wastewater. Process Biochemistry. 2004;39:2035-41.
22. Bai L, Wang C, Pei Y, Zhao J. Reuse of drinking water treatment residuals in a continuous stirred tank reactor for phosphate removal from urban wastewater. Environmental Technology. 2014;35:2752-9.
23. EMIS. Biological nutrient removal, http://emis.vito.be/techniekfiche/biological-nutrient-removal?language=en 2010 [cited 2015 March 3]. Available from: http://emis.vito.be/techniekfiche/biological-nutrient-removal.
24. Yilmaz G, Lemaire R, Keller J, Yuan Z. Simultaneous nitrification, denitrification, and phosphorus removal from nutrient-rich industrial wastewater using granular sludge. Biotechnology and Bioengineering. 2008;100:529-41.

25. Saha B, Chakraborty S, Das G. A mechanistic insight into enhanced and selective phosphate adsorption on a coated carboxylated surface. Journal of Colloid and Interface Science. 2009;331:21-6.
26. de la Noue J, de Pauw N. The potential of microalgal biotechnology: A review of production and uses of microalgae. Biotechnology Advances. 1988;6:725-70.
27. Zelmanov G, Semiat R. The influence of competitive inorganic ions on phosphate removal from water by adsorption on iron (Fe+3) oxide/hydroxide nanoparticles-based agglomerates. Journal of Water Process Engineering. 2014.
28. Qu X, Alvarez PJJ, Li Q. Applications of nanotechnology in water and wastewater treatment. Water Research. 2013;47:3931-46.
29. Savage N, Diallo M. Nanomaterials and Water Purification: Opportunities and Challenges. J Nanopart Res. 2005;7:331-42.
30. Zeng L, Li X, Liu J. Adsorptive removal of phosphate from aqueous solutions using iron oxide tailings. Water Research. 2004;38:1318-26.
31. Zach-Maor A, Semiat R, Shemer H. Synthesis, performance, and modeling of immobilized nano-sized magnetite layer for phosphate removal. Journal of Colloid and Interface Science. 2011;357:440-6.
32. Strauss R, BrÜMmer GW, Barrow NJ. Effects of crystallinity of goethite: II. Rates of sorption and desorption of phosphate. European Journal of Soil Science. 1997;48:101-14.
33. Streat M, Hellgardt K, Newton NLR. Hydrous ferric oxide as an adsorbent in water treatment: Part 3: Batch and mini-column adsorption of arsenic, phosphorus, fluorine and cadmium ions. Process Safety and Environmental Protection. 2008;86:21-30.
34. Oguz E. Removal of phosphate from aqueous solution with blast furnace slag. Journal of Hazardous Materials. 2004;114:131-7.
35. Nowack B, Stone AT. Competitive adsorption of phosphate and phosphonates onto goethite. Water Research. 2006;40:2201-9.
36. Ma J, Zhu L. Simultaneous sorption of phosphate and phenanthrene to inorgano–organo-bentonite from water. Journal of Hazardous Materials. 2006;136:982-8.
37. Luengo C, Brigante M, Avena M. Adsorption kinetics of phosphate and arsenate on goethite. A comparative study. Journal of Colloid and Interface Science. 2007;311:354-60.

38. Luengo C, Brigante M, Antelo J, Avena M. Kinetics of phosphate adsorption on goethite: Comparing batch adsorption and ATR-IR measurements. Journal of Colloid and Interface Science. 2006;300:511-8.
39. Genz A, Kornmüller A, Jekel M. Advanced phosphorus removal from membrane filtrates by adsorption on activated aluminium oxide and granulated ferric hydroxide. Water Research. 2004;38:3523-30.
40. Chitrakar R, Tezuka S, Sonoda A, Sakane K, Ooi K, Hirotsu T. Phosphate adsorption on synthetic goethite and akaganeite. Journal of Colloid and Interface Science. 2006;298:602-8.
41. Ernst M, Sperlich A, Zheng X, Gan Y, Hu J, Zhao X, Wang J, Jekel M. An integrated wastewater treatment and reuse concept for the Olympic Park 2008, Beijing. Desalination. 2007;202:293-301.
42. Sánchez A, Recillas S, Font X, Casals E, González E, Puntes V. Ecotoxicity of, and remediation with, engineered inorganic nanoparticles in the environment. TrAC Trends in Analytical Chemistry. 2011;30:507-16.
43. Recillas S, García A, González E, Casals E, Puntes V, Sánchez A, Font X. Preliminary study of phosphate adsorption onto cerium oxide nanoparticles for use in water purification; nanoparticles synthesis and characterization. Water Science and Technology. 2012;66:503.
44. Gupta VK, Ali I. Chapter 3 - Water Treatment for Organic Pollutants by Adsorption Technology. In: Ali VKG, editor. Environmental Water: Elsevier; 2013. p. 93-116.
45. Ungureanu G, Santos S, Boaventura R, Botelho C. Arsenic and antimony in water and wastewater: Overview of removal techniques with special reference to latest advances in adsorption. Journal of Environmental Management. 2015;151:326-42.
46. Geelhoed JS, Hiemstra T, Van Riemsdijk WH. Phosphate and sulfate adsorption on goethite: Single anion and competitive adsorption. Geochimica et Cosmochimica Acta. 1997;61:2389-96.
47. Wasay SA, Tokunaga S, Park S-W. Removal of Hazardous Anions from Aqueous Solutions by La(lll)- and Y(lll)-lmpregnated Alumina. Separation Science and Technology. 1996;31:1501-14.
48. Zhang L, Gao Y, Li M, Liu J. Expanded graphite loaded with lanthanum oxide used as a novel adsorbent for phosphate removal from water: performance and mechanism study. Environmental Technology. 2015;36:1016-25.

49. Kabayama M, Kawasaki N, Nakamura T, Tanada S. Adsorption/Desorption Characteristics of Phosphate Ion onto Calcined Boehmite Surface. e-Journal of Surface Science and Nanotechnology. 2005;3:63-9.
50. Kabayama M, Sakiyama T, Kawasaki N, Nakamura T, Araki M, Tanada S. Characteristics of Phosphate Ion Adsorption–Desorption onto Aluminum Oxide Hydroxide for Preventing Eutrophication. JOURNAL OF CHEMICAL ENGINEERING OF JAPAN. 2003;36:499-505.
51. Gao S, Wang C, Pei Y. Comparison of different phosphate species adsorption by ferric and alum water treatment residuals. Journal of Environmental Sciences. 2013;25:986-92.
52. Guaya D, Valderrama C, Farran A, Armijos C, Cortina JL. Simultaneous phosphate and ammonium removal from aqueous solution by a hydrated aluminum oxide modified natural zeolite. Chemical Engineering Journal. 2015;271:204-13.
53. Oliveira M, Ribeiro D, Nobrega JM, Machado AV, Brito AG, Nogueira R. Removal of phosphorus from water using active barriers: Al2O3 immobilized on to polyolefins. Environmental Technology. 2011;32:989-95.
54. Wu D, Shen Y, Ding A, Qiu M, Yang Q, Zheng S. Phosphate removal from aqueous solutions by nanoscale zero-valent iron. Environmental Technology. 2013;34:2663-9.
55. Tang J, Chen J, Huang W, Li D, Zhu Y, Tong Y, Zhang Y. Porous Pr(OH)3 nanowires as novel high-performance adsorbents for phosphate removal. Chemical Engineering Journal. 2014;252:202-9.
56. Xu N, Li Y, Zheng L, Gao Y, Yin H, Zhao J, Chen Z, Chen J, Chen M. Synthesis and application of magnesium amorphous calcium carbonate for removal of high concentration of phosphate. Chemical Engineering Journal. 2014;251:102-10.
57. Su Y, Yang W, Sun W, Li Q, Shang JK. Synthesis of mesoporous cerium–zirconium binary oxide nanoadsorbents by a solvothermal process and their effective adsorption of phosphate from water. Chemical Engineering Journal. 2015;268:270-9.
58. Zong E, Wei D, Wan H, Zheng S, Xu Z, Zhu D. Adsorptive removal of phosphate ions from aqueous solution using zirconia-functionalized graphite oxide. Chemical Engineering Journal. 2013;221:193-203.

59. Lin Y-F, Chen H-W, Chen Y-C, Chiou C-S. Application of magnetite modified with polyacrylamide to adsorb phosphate in aqueous solution. Journal of the Taiwan Institute of Chemical Engineers. 2013;44:45-51.
60. Bastin O, Janssens F, Dufey J, Peeters A. Phosphorus removal by a synthetic iron oxide–gypsum compound. Ecological Engineering. 1999;12:339-51.
61. Lakshmanan R, Okoli C, Boutonnet M, Järås S, Rajarao GK. Microemulsion prepared magnetic nanoparticles for phosphate removal: Time efficient studies. Journal of Environmental Chemical Engineering. 2014;2:185-9.
62. Zhang C, Chen L, Wang T-J, Su C-L, Jin Y. Synthesis and properties of a magnetic core–shell composite nano-adsorbent for fluoride removal from drinking water. Applied Surface Science. 2014;317:552-9.
63. Bhaumik M, Leswifi TY, Maity A, Srinivasu VV, Onyango MS. Removal of fluoride from aqueous solution by polypyrrole/Fe3O4 magnetic nanocomposite. Journal of Hazardous Materials. 2011;186:150-9.
64. Tu Y-J, You C-F, Chang C-K, Chen M-H. Application of magnetic nano-particles for phosphorus removal/recovery in aqueous solution. Journal of the Taiwan Institute of Chemical Engineers. 2015;46:148-54.
65. Yang J, Zeng Q, Peng L, Lei M, Song H, Tie B, Gu J. La-EDTA coated Fe3O4 nanomaterial: Preparation and application in removal of phosphate from water. Journal of Environmental Sciences. 2013;25:413-8.
66. Zou C, Gu T, Xiao P, Ge T, Wang M, Wang K. Experimental Study of Cucurbit[7]uril Derivatives Modified Acrylamide Polymer for Enhanced Oil Recovery. Industrial & Engineering Chemistry Research. 2014;53:7570-8.
67. Roy S, Yue CY, Venkatraman SS, Ma LL. Fabrication of smart COC chips: Advantages of N-vinylpyrrolidone (NVP) monomer over other hydrophilic monomers. Sensors and Actuators B: Chemical. 2013;178:86-95.
68. Shin Y, Lee D, Lee K, Ahn KH, Kim B. Surface properties of silica nanoparticles modified with polymers for polymer nanocomposite applications. Journal of Industrial and Engineering Chemistry. 2008;14:515-9.
69. Xiong H-M. Photoluminescent ZnO nanoparticles modified by polymers. Journal of Materials Chemistry. 2010;20:4251-62.

70. DeMarco MJ, SenGupta AK, Greenleaf JE. Arsenic removal using a polymeric/inorganic hybrid sorbent. Water Research. 2003;37:164-76.
71. Cumbal L, Greenleaf J, Leun D, SenGupta AK. Polymer supported inorganic nanoparticles: characterization and environmental applications. Reactive and Functional Polymers. 2003;54:167-80.
72. Onyango MS, Kojima Y, Matsuda H, Ochieng A. Adsorption Kinetics of Arsenic Removal from Groundwater by Iron-Modified Zeolite. JOURNAL OF CHEMICAL ENGINEERING OF JAPAN. 2003;36:1516-22.
73. Katsoyiannis IA, Zouboulis AI. Removal of arsenic from contaminated water sources by sorption onto iron-oxide-coated polymeric materials. Water Research. 2002;36:5141-55.
74. Cumbal L, SenGupta AK. Arsenic Removal Using Polymer-Supported Hydrated Iron(III) Oxide Nanoparticles: Role of Donnan Membrane Effect†. Environ Sci Technol. 2005;39:6508-15.
75. Zhang Y, Pan B. Modeling batch and column phosphate removal by hydrated ferric oxide-based nanocomposite using response surface methodology and artificial neural network. Chemical Engineering Journal. 2014;249:111-20.
76. You X, Guaya D, Farran A, Valderrama C, Cortina JL. Phosphate removal from aqueous solution using a hybrid impregnated polymeric sorbent containing hydrated ferric oxide (HFO). Journal of Chemical Technology & Biotechnology. 2015:n/a-n/a.
77. Pan B, Wu J, Pan B, Lv L, Zhang W, Xiao L, Wang X, Tao X, Zheng S. Development of polymer-based nanosized hydrated ferric oxides (HFOs) for enhanced phosphate removal from waste effluents. Water Research. 2009;43:4421-9.
78. Blaney LM, Cinar S, SenGupta AK. Hybrid anion exchanger for trace phosphate removal from water and wastewater. Water Research. 2007;41:1603-13.
79. Yang W, Yu Z, Pan B, Lv L, Zhang W. Simultaneous organic/inorganic removal from water using a new nanocomposite adsorbent: A case study of p-nitrophenol and phosphate. Chemical Engineering Journal. 2015;268:399-407.
80. Abo-Farha SA, Abdel-Aal AY, Ashour IA, Garamon SE. Removal of some heavy metal cations by synthetic resin purolite C100. Journal of Hazardous Materials. 2009;169:190-4.
81. Liu C, Huang PM. Kinetics of phosphate adsorption on iron oxides formed under the influence of citrate. Canadian Journal of Soil Science. 2000;80:445-54.

82. Colombo C, Barrón V, Torrent J. Phosphate adsorption and desorption in relation to morphology and crystal properties of synthetic hematites. Geochimica et Cosmochimica Acta. 1994;58:1261-9.
83. Alonso A, Vigues N, Munoz-Berbel X, Macanas J, Munoz M, Mas J, Muraviev DN. Environmentally-safe bimetallic Ag@Co magnetic nanocomposites with antimicrobial activity. Chemical Communications. 2011;47:10464-6.
84. Alonso A. Development of polymeric nanocomposites with enhanced distribution of catalytically active or bactericide nanoparticles. 2012.
85. Alonso A, Shafir A, Macanás J, Vallribera A, Muñoz M, Muraviev DN. Recyclable polymer-stabilized nanocatalysts with enhanced accessibility for reactants. Catalysis Today. 2012;193:200-6.
86. Dorado AD, Gamisans X, Valderrama C, Solé M, Lao C. Cr(III) removal from aqueous solutions: A straightforward model approaching of the adsorption in a fixed-bed column. Journal of Environmental Science and Health, Part A. 2013;49:179-86.
87. Nur T, Johir MAH, Loganathan P, Nguyen T, Vigneswaran S, Kandasamy J. Phosphate removal from water using an iron oxide impregnated strong base anion exchange resin. Journal of Industrial and Engineering Chemistry. 2014;20:1301-7.
88. Vente JA, Bosch H, de Haan AB, Bussmann PJT. Evaluation of sugar sorption isotherm measurement by frontal analysis under industrial processing conditions. Journal of Chromatography A. 2005;1066:71-9.
89. Dorado AD, Lafuente J, Gabriel D, Gamisans X. The role of water in the performance of biofilters: Parameterization of pressure drop and sorption capacities for common packing materials. Journal of Hazardous Materials. 2010;180:693-702.
90. Lemine OM, Omri K, Zhang B, El Mir L, Sajieddine M, Alyamani A, Bououdina M. Sol–gel synthesis of 8 nm magnetite (Fe3O4) nanoparticles and their magnetic properties. Superlattices and Microstructures. 2012;52:793-9.
91. Neyaz N, Zarger MSS, Siddiqui WA. Synthesis and characterisation of modified magnetite super paramagnetic nano composite for removal of toxic metals from ground water. International Journal of Environmental Sciences. 2014;5:260-9.

92. Farghali MA, El-Din TAS, Al-Enizi AM, Bahnasawy RME. Graphene/ Magnetite Nanocomposite for Potential Environmental Application. Int J Electrochem Sci. 2015;10:529 - 37.
93. Ahn J-H, Jang J-E, Oh C-G, Ihm S-K, Cortez J, Sherrington DC. Rapid Generation and Control of Microporosity, Bimodal Pore Size Distribution, and Surface Area in Davankov-Type Hyper-Cross-Linked Resins. Macromolecules. 2006;39:627-32.
94. Rodrigues L, da Silva M. Adsorption kinetic, thermodynamic and desorption studies of phosphate onto hydrous niobium oxide prepared by reverse microemulsion method. Adsorption. 2010;16:173-81.
95. Zeng H, Fisher B, Giammar DE. Individual and competitive adsorption of arsenate and phosphate to a high-surface-area iron oxide-based sorbent. Environmental Science and Technology. 2008;42:147-52.
96. Krishnan KA, Haridas A. Removal of phosphate from aqueous solutions and sewage using natural and surface modified coir pith. Journal of Hazardous Materials. 2008;152:527-35.
97. Das J, Patra BS, Baliarsingh N, Parida KM. Adsorption of phosphate by layered double hydroxides in aqueous solutions. Applied Clay Science. 2006;32:252-60.
98. Kim J, Li W, Philips BL, Grey CP. Phosphate adsorption on the iron oxyhydroxides goethite ([small alpha]-FeOOH), akaganeite ([small beta]-FeOOH), and lepidocrocite ([gamma]-FeOOH): a 31P NMR Study. Energy & Environmental Science. 2011;4:4298-305.